arXiv:1704.03211v1 [quant-ph] 11 Apr 2017

The quantum Rabi model in a superfluid Bose-Einstein condensate

S. Felicetti[1,*], G. Romero[2], E. Solano[3,4], and C. Sabín[5]

[1]Laboratoire Matériaux et Phénomènes Quantiques, Sorbonne Paris Cité, Université Paris Diderot, CNRS UMR 7162, 75013, Paris, France
[2]Departamento de Física, Universidad de Santiago de Chile (USACH), Avenida Ecuador 3493, 9170124, Santiago, Chile
[3]Department of Physical Chemistry, University of the Basque Country UPV/EHU, Apartado 644, E-48080 Bilbao, Spain
[4]IKERBASQUE, Basque Foundation for Science, Maria Diaz de Haro 3, 48013 Bilbao, Spain
[5]Instituto de Física Fundamental, CSIC, Serrano 113-bis 28006 Madrid, Spain
[*]felicetti.simone@gmail.com

ABSTRACT

We propose a quantum simulation of the quantum Rabi model in an atomic quantum dot, which is a single atom in a tight optical trap coupled to the quasiparticle modes of a superfluid Bose-Einstein condensate. This widely tunable setup allows to simulate the ultrastrong coupling regime of light-matter interaction in a system which enjoys an amenable characteristic timescale, paving the way for an experimental analysis of the transition between the Jaynes-Cummings and the quantum Rabi dynamics using cold-atom systems. Our scheme can be naturally extended to simulate multi-qubit quantum Rabi models. In particular, we discuss the appearance of effective two-qubit interactions due to phononic exchange, among other features.

Introduction

The engineering of light-matter interaction lies at the core of modern quantum science. Its development has allowed us to implement highly controllable quantum technologies where atomic or solid-state systems interact with confined modes of the electromagnetic field. Physical implementations include cavity quantum electrodynamics (QED)[1,2], ultracold atoms[3], trapped ions[4], hybrid systems[5], and circuit QED[6–9]. A turning point in the history of quantum technologies has been marked by the achievement of the strong coupling (SC) regime[10,11], where the interaction strength overcomes dissipation rates. In the SC regime, coherent quantum processes can be observed and even applied in quantum information tasks.

When the light-matter interaction strength becomes comparable with the systems bare frequencies, the ultrastrong coupling (USC) regime[12,13] is reached, where the system spectrum and dynamical features are fundamentally modified. The minimal model of light-matter interaction is called quantum Rabi model[14] (QRM), and it consists of a two-level quantum system (qubit) coupled with a single bosonic mode. In spite of its apparent simplicity, the dynamics of the QRM in the USC regime cannot be solved analytically, and its eigenspectrum has been obtained only recently[15]. The USC regime has been experimentally observed using semiconductor quantum wells[16–18], molecular cavity QED[19,20] and superconducting quantum circuits[21–23]. Recently, the latter technology allowed to couple matter excitations with a continuum of bosonic modes[24], or with extreme values of the coupling strength[25], a condition called deep strong coupling (DSC) regime. The growing interest on the USC regime is motivated not only by its fundamental features, but also by potential quantum-information applications, such as parity-protected quantum computation[26,27], quantum information storage[28], and ultrafast quantum information processing[29].

Although exciting, natural implementations of systems in the USC regime are still very challenging and they are confined by fundamental limitations. However, using quantum-simulation schemes, the physics of the USC regime can be observed also in systems that do not naturally achieve this regime of interaction[30–36]. These techniques allow to explore all parameter regimes, to overcome fundamental limitations and to observe exotic interactions. In particular, different schemes have been proposed to implement the QRM using superconducting circuits[30], quantum optical systems[31], trapped ions[32] and cold atoms[36]. An experimental simulation of the QRM has been recently implemented[34], using a digital quantum simulation scheme on superconducting quantum devices.

In this work, we propose an alternative setup for the quantum simulation of the quantum Rabi model in a cold atom system, see Fig. 1. The proposed scheme consists of a superfluid Bose-Einstein condensate (BEC) in a shallow confining trap, where an atomic quantum dot interacts with phononic quasiparticle modes of the BEC. All the parameters can be widely tuned, allowing to observe the transition between strong, ultrastrong and deep strong coupling regime. Furthermore, due to the slow speed

of propagation of the quasiparticles, the characteristic frequencies of this setup can be as low as several Hz, resulting in a favourable timescale for real-time control of the artificial matter-radiation interaction. Therefore, our setup offers a promising testbed for the experimental analysis of the full quantum Rabi model (QRM)[14,15]. Moreover, our scheme allows to implement a controllable interaction between atomic quantum dots, mediated by dispersive coupling with phononic modes. In this case, the possibility to reach the USC regime provides an effective qubit-qubit interaction[37] that is robust against thermal effects[38].

Quantum simulation scheme

The system here considered consists in a Bose-Einstein condensate (BEC) superfluid reservoir in a shallow confining trap and one or more two-level quantum systems (TLSs). One possible implementation of a TLS is an atomic quantum dot[39–41]. The dot is created by applying a localized steep potential which traps atoms of a different hyperfine state and of the same atomic species as the BEC. We will use a and b to denote atoms in the BEC and the dot traps respectively. We consider the collisional blockade regime, requiring the interactions between atoms in the dot to be much larger than the interactions between atoms in the condensate reservoir $g_{bb} \gg g_{aa}$, so that the dot occupation number can only be 0 or 1, giving rise to a TLS. Alternatively, in reference[42] the TLSs are created by loading cold atoms of a different species in an optical lattice consisting of double-well potentials where only single occupancy of each site is allowed.

We consider the BEC reservoir in the low temperature superfluid regime, in which the density of the condensate can be split into a background mean-field term and a quantum fluctuation operator $\Pi(\mathbf{x})$, that can be expanded in terms of Bogoliubov modes. For frequencies below a cutoff frequency ω_c, given by the condensate healing length, these modes describe phononic excitations,

$$\Pi(x) = \sum_k \sqrt{N\omega_k}\left[e^{ikx}a_k + \text{H.c.}\right]. \tag{1}$$

This field is described by a continuum of bosonic modes, each described by creation and annihilation Fock operators that satisfy the commutation relation $[a_k, a_{k'}^\dagger] = \delta_{kk'}$, and a linear spectrum, $\omega_k = v|k|$, where v is the propagation velocity of the phononic excitations, given by $mv^2 = \rho_a g_{aa}$ in a weakly interacting BEC. Here, m and ρ_a are the mass of bosons in the condensate and the condensate density, respectively. The coupling strength g_{aa} is expressed as $g_{aa} = 4\pi\hbar^2 a_{aa}/m$, where a_{aa} the scattering length of atoms in the BEC. Therefore, the speed of sound in the BEC is proportional to the square root of the scattering length, which can be controlled by tuning an external magnetic field around a Feshbach resonance[43–45]. Finally, N is a normalization constant $N = \hbar/(2V g_{aa})$, that depends on the condensate volume V. The dots are coupled to the condensate reservoir through a Raman transition of effective Rabi frequency Ω and detuning δ by means of external lasers, which give rise to a phonon-mediated interaction.

Within the above approximations, the system is well described by a spin-boson like Hamiltonian,

$$\begin{aligned} H &= \left(\frac{\hbar\Omega_d}{2}\sigma^z + \left[-\delta' + \sum_{\mathbf{k}} g\left(a_{\mathbf{k}} + a_{\mathbf{k}}^\dagger\right)\right]\frac{\hbar\sigma^x}{2}\right) + \\ &+ \sum_{\mathbf{k}} \hbar\omega_{\mathbf{k}} a_{\mathbf{k}}^\dagger a_{\mathbf{k}}\,, \end{aligned} \tag{2}$$

where σ_x, σ_z are Pauli spin matrices. The first term in Eq.(2) is the free Hamiltonian of an effective qubit with energy gap $\hbar\Omega_d$. The frequency Ω_d is determined by the effective Rabi frequency Ω of the Raman transition and the number of atoms in the condensate. The second term describes the coupling of the dot with the phononic field, whose Hamiltonian is given by the third term in Eq. (2). The dot-phonon coupling is characterized by

$$g = \sqrt{\frac{N\omega_k}{\hbar^2}}\left(g_{ab} - g_{aa}\right). \tag{3}$$

Here, g_{ab} is the coupling strength between the dot and condensate atoms, given by $g_{ab} = 4\pi\hbar^2 a_{ab}/m$. δ' is dependent on g_{ab}, g_{aa}, Ω and δ[39]. As all the coupling strengths, g_{ab}, g_{aa} and g_{bb}, can be tuned by Feshbach resonances, and we are able to consider the case $\delta' = 0$. In this case, the interaction Hamiltonian for a single dot can be rewritten as:

$$H_I = \hbar(g_{ab} - g_{aa})\Pi(\mathbf{x}_a). \tag{4}$$

With suitable boundary conditions for the condensate trap, e. g. hard-wall or box potentials[46–48], the energy separation of the phononic modes can be large enough to ensure that each TLS is only effectively coupled to the mode with closest frequency to

Ω_d. We denote this frequency by Ω_f. In a 3D condensate, taking $V = L^3$, $L = 10\,\mu$m and $v = 10$ mm/s , the frequency of the lowest-energy phonons is $\Omega_f \simeq 2\pi \times c/(2L) \simeq 2\pi \times 500$ Hz. For instance, we can consider a K-Rb mixture, where Rb is the atomic species of the condensate and K that of the impurities. Then, the scattering length $a_{\mathrm{RbRb}} = a_{aa} = 102\,a_0$ and $a_{KRb} = a_{ab}$ can be tuned near the Feshbach resonance from $a_{ab} \simeq a_{aa}$ to $a_{ab} > 30\,a_{aa}$[49]. Then g can be tuned within a broad range from $2\pi \times 5$ Hz to $2\pi \times 100$ Hz. In lower dimensions, the value of g can be larger. For instance, if we consider a cylindrical quasi 1D BEC with tight radial confinement $L_r \ll L_z = L$, we have to replace V by L in Eq. (3), and the couplings g_{ij} by $g_{ij}^{(1D)} = g/L_r^2$[50]. Therefore, we obtain $g^{(1D)} = \lambda^{-1/2} g$, where $\lambda = (L_r/L_z)^2 \ll 1$ is the aspect ratio of the condensate. With a typical value $\lambda \simeq 10^{-3}$[51], we get $g^{(1D)} \simeq 30\,g$.

The readout can be performed including additional atomic quantum dots coupled to the BEC in the dispersive regime. In this way, the effective qubit can be used to realize a quantum non-demolition measurement of the average number of phonons. Recently, some of us have shown indeed that this setup can be used as a highly sensitive thermometer at ultralow temperatures, which in turn amounts to measure the average number of phonons in a field mode[52]. Remarkably, a large number of independent atomic quantum dots can be used. Alternatively, an optical lattice loaded with cold atoms in the single occupancy regime would give rise to a similar model[42].

It is worth mention that our setup is different from other possible implementation of the QRM in cold-atoms systems. In a spin-orbit coupled condensate[53,54] two-level systems are encoded in internal atomic hyperfine levels of the Raman-dressed condensate, while the bosonic mode refers to the atomic wavefunction in a harmonic trap, that is not to the quasiparticle modes. This configuration allows to observe impressive many-body phenomena, but it cannot be applied to implement few-body interactions in the USC regime. A scheme to implement the QRM in cold atoms systems has also been proposed[36], where both the qubit and the bosonic mode are encoded in the motion of the atomic cloud in tailored optical lattices[55,56]. This proposal was designed to selectively implement a novel region of parameters in the DSC regime that was previously unexplored, and which could not be accessed by other means.

The quantum Rabi model

The above analysis shows that the USC and DSC regimes of interaction can indeed be achieved. In the following, we will focus on the single-qubit case, and we will address the changes of the system dynamics as the interaction strength is increased. In this case, the system dynamics is governed by the QRM according to the Hamiltonian

$$H_{\mathrm{QRM}} = \frac{\hbar\Omega_d}{2}\sigma^z + \hbar\Omega_f a^\dagger a + \hbar g\sigma^x(a + a^\dagger). \tag{5}$$

A critical issue in the proposed implementation is the cooling of the bosonic excitations. In order to observe Rabi oscillations between the TLS and the bosonic field, the latter must be initialized in the vacuum or in a few-phonon state. To this end, the initial temperature should be low enough to ensure that the average number of thermal excitations in the relevant range of frequencies is close to 0. At 500 Hz, this number is below 10^{-1} at $T = 10$ nK. Temperatures of 0.5 nK has been achieved in a BEC[57]. We have performed numerical simulations in order to analyze interesting dynamics that could be implemented with feasible physical parameters, including the effect of finite-temperature initialization of the bosonic field. The dissipation in the bosonic mode with bare decay parameter γ and temperature has been taken into account by means of the microscopic master equation[58].

Strong to Ultrastrong coupling transition

First, let us consider the transition from the strong to the USC regime. When the coupling strength is small compared to the system frequencies, the quantum Rabi Hamiltonian (5) can be approximated, via rotating-wave approximation, to the Jaynes-Cummings Hamiltonian

$$H_{\mathrm{JC}} = \frac{\hbar\Omega_d}{2}\sigma^z + \hbar\Omega_f a^\dagger a + \hbar g(\sigma^+ a + \sigma^- a^\dagger). \tag{6}$$

In this case, the Hamiltonian respects a continuous $U(1)$ symmetry that preserves the total number of excitations $\hat{N} = a^\dagger a + \sigma^+\sigma^-$. The system dynamics consists in coherent exchange of excitations between the TLS and the field, dubbed Rabi oscillations. As the coupling strength increases and the system reaches the USC regime, the full QRM of Eq.(5) must be considered, and the continuous symmetry breaks down into a discrete $\mathbb{Z}_2$-symmetry, defined by the parity operator $\hat{P} = -\sigma^z e^{i\pi a^\dagger a}$. Accordingly, the number of excitations is not conserved, and the parity symmetry sets selection rules for state transitions[27,59]. The transition from the SC to the USC regime entails fundamental modification to the system ground state, which is not the vacuum but contains virtual photons. As a result, the uncoupled basis of phonons and TLS excitations does not provide an intuitive description of the system dynamics.

To illustrate this transition, we have simulated the system dynamics taking as initial state the qubit excited state and a thermal state for the phonon field $\rho(0) = |\downarrow\rangle\langle\downarrow| \otimes \rho_{\text{thermal}}$. Fig. 2 shows the average phonon number N_{ph} and Fig. 3 the population inversion S_z as a function of time, for different values of the coupling strength. As the coupling g is increased, the Jaynes-Cummings evolution is replaced by a less intuitive dynamics. The feasible physical parameters here considered allow to observe the transition from a dynamics dominated by Rabi oscillations Fig.2(a) (Fig.3(a)), to a dynamics that does not preserve the excitation number Fig.2(b) (Fig.3(b)) and, finally, to the fast generation of phonon excitations Fig.2(c) (Fig.3(c)).

Collapses and revivals

When the interaction strength is increase further, and it becomes even larger than the field and TLS frequencies, the system enters the DSC regime[60]. The most peculiar feature of this regime consists in collapses and revivals of the initial states $|\downarrow,0\rangle$ ($|\uparrow,0\rangle$), i.e., when the field is initialized in the vacuum state and the qubit in the ground (excited) state of its free Hamiltonian term $\hbar\Delta\sigma_z$. Notice that in the USC and DSC regimes, the ground state is not the vacuum anymore, but it is given by an entangled state that contains virtual phonons and TLS excitations. This means that the state $|\downarrow,0\rangle$ is actually an excited one, and it is non-trivial to generate in natural implementation of the QRM. In order to initialize the system in such a state, we can take profit of the tunability of the coupling strength provided by the present scheme as it follows. First, he system is initialized in the strong coupling regime and cooled close to its ground state. Then, the effective interaction strength is suddenly switched to the desired value in the USC or DSC range. To this end, the magnetic field must be changed near a Feshbach resonance, to jump from $g = 0$ ($g_{ab} = g_{aa}$) to the values such that g ($g_{ab} > g_{aa}$), in the sub-milisecond regime. In the case of K-Rb mixture, a magnetic field change of less than of 1 G is enough[49] to span the interesting range of interaction strength. It has been experimentally proven that such a quench can be achieved in less than 1 ms in a controlled fashion[61].

We have implemented numerical simulations to verify the impact on collapses and revivals of finite temperature effects, that is imperfect state preparation and amplified dissipation. In Fig. 4 it is shown the probability $P_{\downarrow,0}(t) = |\langle\downarrow,0|\psi(t)\rangle|^2$ as a function of time and for three different temperatures. The initial condition is chosen as $\rho(0) = |\downarrow\rangle\langle\downarrow| \otimes \rho_{\text{thermal}}$, that is the qubit in its ground state and the phononic mode in a low-excited thermal state. The dynamics exhibits oscillations coming from the phonon-number wave packet that spread along the parity basis $p = +1$ ($\hat{P}|\downarrow,0\rangle = +|\downarrow,0\rangle$)[60]. For all cases we have considered $g/\Omega_f = 0.8$, and $\Omega_d/\Omega_f = 0.1$. As shown by the blue line with squared markers in Fig. 4, collapses and revivals are still visible also at $T = 20$ nK.

Effective two-body interactions.

Let us now extend our model to consider n quantum dots coupled with a single phononic mode. In this case the system Hamiltonian is given by a multi-qubit quantum Rabi model, known as Dicke model in the many-body case,

$$H = \hbar \sum_{n=1}^{n} \frac{\Omega_{dn}}{2}\sigma_n^z + \hbar\Omega_f a^\dagger a + \hbar \sum_{n=1}^{n} g_n \sigma_n^x (a + a^\dagger). \tag{7}$$

In the dispersive regime, where the qubits are off-resonance with respect to the bosonic mode, the system dynamics results in an effective interactions between the qubits. This condition can be used to implement quantum gates[62] or quantum simulations of spin chains[63]. Here we consider the case where the interaction strength is large enough to break the rotating-wave approximation, even in the dispersive limit[37]. Such interaction leads to an effective Ising-type interaction between atomic quantum dots mediated by a single phononic mode, and single-mode squeezing upon the latter. This effective interaction can be obtained from the Hamiltonian of Eq. (7) by applying a Schrieffer-Wolf transformation $e^S H e^{-S}$[64], with $S = \sum_n [(g_n/\Delta_n)(\sigma_n^+ a - \sigma_n^- a^\dagger) + (g_n/\delta_n)(\sigma_n^+ a^\dagger - \sigma_n^- a)]$. As shown in Ref.[37], the above transformation leads to the effective Hamiltonian

$$H_{\text{eff}} = \hbar\Omega_f a^\dagger a + \hbar \sum_{n=1}^{n} \frac{\Omega_{dn}}{2}\sigma_n^z + \frac{\hbar}{2} \sum_{n=1}^{n} g_n^2 \left(\frac{1}{\Delta_n} + \frac{1}{\delta_n}\right)(a + a^\dagger)^2 \sigma_n^z + \frac{\hbar}{2} \sum_{n>m} J_{nm} \sigma_n^x \sigma_m^x, \tag{8}$$

where the effective coupling strengths are defined as

$$J_{nm} = g_n g_m \left(\frac{1}{\Delta_n} + \frac{1}{\Delta_m} - \frac{1}{\delta_n} - \frac{1}{\delta_m}\right), \tag{9}$$

and $\Delta_n = \Omega_{dn} - \Omega_f$ and $\delta_n = \Omega_{dn} + \Omega_f$.

We have performed numerical simulations to check the validity of this approximation at finite temperature. In Fig. 5 we show the results obtained comparing the dynamics of the full (7) and effective (8)] Hamiltonian. The plots show the

exchange of excitations between two identical qubits as function of time, when the initial condition is given by $\rho(0) = |\uparrow\rangle\langle\uparrow| \otimes |\downarrow\rangle\langle\downarrow| \otimes \rho_{\text{thermal}}$, for different temperatures of the bosonic mode. The effective Hamiltonian describes accurately the system dynamics for low temperatures [see Fig. 5(a)]. When significant thermal effects are included, as in Fig. 5(b), small oscillation at a fasters timescale appear, but the effective model still provides a qualitative description of the excitation exchange.

Conclusions

We propose a novel scheme to implement a quantum simulation of the quantum Rabi model in a cold-atom setup. It consists of an atomic quantum dot coupled to the quasiparticle excitations of a BEC with suitable hard-wall boundary conditions. By exploiting the dependence of the atomic collision strengths on external magnetic fields near a Feshbach resonance, the parameters of the condensate can be tuned over a wide interval spanning the SC, USC and DSC regime of interaction. An important feature of our setup is the slow propagation speed of the quasiparticles whose characteristic frequencies are in the of tens or hundreds of Hz. This results in a slow time scale that facilitates the experimental preparation of the initial states and the control of the interaction strength required to analyze the features of the quantum Rabi model. Our scheme can be naturally extended including additional two-level systems. We have analyzed the appearance of effective phonon-mediated pairwise interactions. Our scheme would allow to experimentally investigate the effect of finite temperature on dispersively-coupled qubits in the transition between the strong and the ultrastrong coupling regimes.

References

1. Walther, H., Varcoe, B. T., Englert, B.-G. & Becker, T. Cavity quantum electrodynamics. *Reports on Prog. Phys.* **69**, 1325 (2006).
2. Raimond, J.-M. & Haroche, S. *Exploring the quantum* (Oxford University Press, Oxford, 2006).
3. Greiner, M., Mandel, O., Esslinger, T., Hänsch, T. W. & Bloch, I. Quantum phase transition from a superfluid to a mott insulator in a gas of ultracold atoms. *Nat.* **415**, 39–44 (2002).
4. Leibfried, D., Blatt, R., Monroe, C. & Wineland, D. Quantum dynamics of single trapped ions. *Rev. Mod. Phys.* **75**, 281 (2003).
5. Xiang, Z.-L., Ashhab, S., You, J. & Nori, F. Hybrid quantum circuits: Superconducting circuits interacting with other quantum systems. *Rev. Mod. Phys.* **85**, 623 (2013).
6. Blais, A., Huang, R.-S., Wallraff, A., Girvin, S. M. & Schoelkopf, R. J. Cavity quantum electrodynamics for superconducting electrical circuits: An architecture for quantum computation. *Phys. Rev. A* **69**, 062320 (2004).
7. Wallraff, A. *et al.* Strong coupling of a single photon to a superconducting qubit using circuit quantum electrodynamics. *Nat.* **431**, 162–167 (2004).
8. Chiorescu, I. *et al.* Coherent dynamics of a flux qubit coupled to a harmonic oscillator. *Nat.* **431**, 159–162 (2004).
9. Devoret, M. H. & Schoelkopf, R. J. Superconducting circuits for quantum information: an outlook. *Sci.* **339**, 1169–1174 (2013).
10. Haroche, S. Nobel lecture: Controlling photons in a box and exploring the quantum to classical boundary. *Rev. Mod. Phys.* **85**, 1083 (2013).
11. Wineland, D. J. Nobel lecture: Superposition, entanglement, and raising schrödinger's cat. *Rev. Mod. Phys.* **85**, 1103 (2013).
12. Ciuti, C., Bastard, G. & Carusotto, I. Quantum vacuum properties of the intersubband cavity polariton field. *Phys. Rev. B* **72**, 115303 (2005).
13. Ciuti, C. & Carusotto, I. Input-output theory of cavities in the ultrastrong coupling regime: The case of time-independent cavity parameters. *Phys. Rev. A* **74**, 033811 (2006).
14. Rabi, I. On the process of space quantization. *Phys. Rev.* **49**, 324 (1936).
15. Braak, D. Integrability of the rabi model. *Phys. Rev. Lett.* **107**, 100401 (2011).
16. Anappara, A. A. *et al.* Signatures of the ultrastrong light-matter coupling regime. *Phys. Rev. B* **79**, 201303 (2009).
17. Günter, G. *et al.* Sub-cycle switch-on of ultrastrong light–matter interaction. *Nat.* **458**, 178–181 (2009).
18. Todorov, Y. *et al.* Ultrastrong light-matter coupling regime with polariton dots. *Phys. Rev. Lett.* **105**, 196402 (2010).
19. Schwartz, T., Hutchison, J. A., Genet, C. & Ebbesen, T. W. Reversible switching of ultrastrong light-molecule coupling. *Phys. Rev. Lett.* **106**, 196405 (2011).

20. George, J. *et al.* Multiple rabi splittings under ultrastrong vibrational coupling. *Phys. Rev. Lett.* **117**, 153601 (2016).

21. Bourassa, J. *et al.* Ultrastrong coupling regime of cavity QED with phase-biased flux qubits. *Phys. Rev. A* **80**, 032109 (2009).

22. Niemczyk, T. *et al.* Circuit quantum electrodynamics in the ultrastrong-coupling regime. *Nat. Phys.* **6**, 772–776 (2010).

23. Forn-Díaz, P. *et al.* Observation of the bloch-siegert shift in a qubit-oscillator system in the ultrastrong coupling regime. *Phys. Rev. Lett.* **105**, 237001 (2010).

24. Forn-Díaz, P. *et al.* Ultrastrong coupling of a single artificial atom to an electromagnetic continuum in the nonperturbative regime. *Nat. Phys.* **13**, 39–43 (2017).

25. Yoshihara, F. *et al.* Superconducting qubit-oscillator circuit beyond the ultrastrong-coupling regime. *Nat. Phys.* **13**, 44–47 (2017).

26. Nataf, P. & Ciuti, C. Protected quantum computation with multiple resonators in ultrastrong coupling circuit QED. *Phys. Rev. Lett.* **107**, 190402 (2011).

27. Felicetti, S., Douce, T., Romero, G., Milman, P. & Solano, E. Parity-dependent state engineering and tomography in the ultrastrong coupling regime. *Sci. Reports* **5**, 11818 (2015).

28. Kyaw, T., Felicetti, S., Romero, G., Solano, E. & Kwek, L. Scalable quantum random-access memory with superconducting circuits. *Sci. Reports* **5**, 8621 (2015).

29. Romero, G., Ballester, D., Wang, Y., Scarani, V. & Solano, E. Ultrafast quantum gates in circuit QED. *Phys. Rev. Lett.* **108**, 120501 (2012).

30. Ballester, D., Romero, G., García-Ripoll, J. J., Deppe, F. & Solano, E. Quantum simulation of the ultrastrong-coupling dynamics in circuit quantum electrodynamics. *Phys. Rev. X* **2**, 021007 (2012).

31. Crespi, A., Longhi, S. & Osellame, R. Photonic realization of the quantum rabi model. *Phys. Rev. Lett.* **108**, 163601 (2012).

32. Pedernales, J. *et al.* Quantum rabi model with trapped ions. *Sci. Reports* **5** (2015).

33. Felicetti, S. *et al.* Spectral collapse via two-phonon interactions in trapped ions. *Phys. Rev. A* **92**, 033817 (2015).

34. Langford, N. *et al.* Experimentally simulating the dynamics of quantum light and matter at ultrastrong coupling. *arXiv preprint arXiv:1610.10065* (2016).

35. Fedortchenko, S. *et al.* Quantum simulation of ultrastrongly coupled bosonic modes using superconducting circuits. *arXiv preprint arXiv:1612.05542* (2016).

36. Felicetti, S. *et al.* Quantum rabi model in the brillouin zone with ultracold atoms. *Phys. Rev. A* **95**, 013827 (2017).

37. Zueco, D., Reuther, G. M., Kohler, S. & Hänggi, P. Qubit-oscillator dynamics in the dispersive regime: Analytical theory beyond the rotating-wave approximation. *Phys. Rev. A* **80**, 033846 (2009).

38. Cárdenas-López, F., Albarrán-Arriagada, F., Barrios, G. A., Retamal, J. & Romero, G. Incoherent-mediator for quantum state transfer in the ultrastrong coupling regime. *arXiv preprint arXiv:1612.06806* (2016).

39. Recati, A., Fedichev, P., Zwerger, W., Von Delft, J. & Zoller, P. Atomic quantum dots coupled to a reservoir of a superfluid bose-Einstein condensate. *Phys. Rev. Lett.* **94**, 040404 (2005).

40. Orth, P. P., Stanic, I. & Le Hur, K. Dissipative quantum ising model in a cold-atom spin-boson mixture. *Phys. Rev. A* **77**, 051601 (2008).

41. Marino, J., Recati, A. & Carusotto, I. Casimir forces and quantum friction from ginzburg radiation in atomic becs. *arXiv preprint arXiv:1605.07642* (2016).

42. Cirone, M., De Chiara, G., Palma, G. & Recati, A. Collective decoherence of cold atoms coupled to a bose-Einstein condensate. *New J. Phys.* **11**, 103055 (2009).

43. Simoni, A. *et al.* Near-threshold model for ultracold KRb dimers from interisotope feshbach spectroscopy. *Phys. Rev. A* **77**, 052705 (2008).

44. Tung, S.-K. *et al.* Ultracold mixtures of atomic 6 Li and 133 Cs with tunable interactions. *Phys. Rev. A* **87**, 010702 (2013).

45. Chin, C. *et al.* Precision feshbach spectroscopy of ultracold Cs 2. *Phys. Rev. A* **70**, 032701 (2004).

46. Hänsel, W., Hommelhoff, P., Hänsch, T. & Reichel, J. Bose–Einstein condensation on a microelectronic chip. *Nat.* **413**, 498–501 (2001).

47. Meyrath, T., Schreck, F., Hanssen, J., Chuu, C.-S. & Raizen, M. Bose-Einstein condensate in a box. *Phys. Rev. A* **71**, 041604 (2005).

48. Gaunt, A. L., Schmidutz, T. F., Gotlibovych, I., Smith, R. P. & Hadzibabic, Z. Bose-Einstein condensation of atoms in a uniform potential. *Phys. Rev. Lett.* **110**, 200406 (2013).

49. Modugno, G., Modugno, M., Riboli, F., Roati, G. & Inguscio, M. Two atomic species superfluid. *Phys. Rev. Lett.* **89**, 190404 (2002).

50. Pitaevskii, L. & Stringari, S. Bose-Einstein condensation (international series of monographs on physics) (2003).

51. Haller, E. *et al.* Confinement-induced resonances in low-dimensional quantum systems. *Phys. Rev. Lett.* **104**, 153203 (2010).

52. Sabín, C., White, A., Hackermuller, L. & Fuentes, I. Impurities as a quantum thermometer for a bose-Einstein condensate. *Sci. Reports* **4** (2014).

53. Zhang, Y., Chen, G. & Zhang, C. Tunable spin-orbit coupling and quantum phase transition in a trapped bose-Einstein condensate. *Sci. Reports* **3**, 1937–1937 (2012).

54. Hamner, C. *et al.* Dicke-type phase transition in a spin-orbit-coupled bose-Einstein condensate. *Nat. Commun.* **5** (2014).

55. Witthaut, D., Salger, T., Kling, S., Grossert, C. & Weitz, M. Effective Dirac dynamics of ultracold atoms in bichromatic optical lattices. *Phys. Rev. A* **84**, 033601 (2011).

56. Salger, T., Grossert, C., Kling, S. & Weitz, M. Klein tunneling of a quasirelativistic bose-Einstein condensate in an optical lattice. *Phys. Rev. Lett.* **107**, 240401 (2011).

57. Leanhardt, A. *et al.* Cooling bose-Einstein condensates below 500 picokelvin. *Sci.* **301**, 1513–1515 (2003).

58. Carusotto, I. *et al.* Fermionized photons in an array of driven dissipative nonlinear cavities. *Phys. Rev. Lett.* **103**, 033601 (2009).

59. Forn-Díaz, P., Romero, G., Harmans, C., Solano, E. & Mooij, J. Broken selection rule in the quantum rabi model. *Sci. Reports* **6** (2016).

60. Casanova, J., Romero, G., Lizuain, I., García-Ripoll, J. J. & Solano, E. Deep strong coupling regime of the jaynes-cummings model. *Phys. Rev. Lett.* **105**, 263603 (2010).

61. Schneider, U. *et al.* Fermionic transport and out-of-equilibrium dynamics in a homogeneous hubbard model with ultracold atoms. *Nat. Phys.* **8**, 213–218 (2012).

62. DiCarlo, L. *et al.* Demonstration of two-qubit algorithms with a superconducting quantum processor. *Nat.* **460**, 240–244 (2009).

63. Majer, J. *et al.* Coupling superconducting qubits via a cavity bus. *Nat.* **449**, 443–447 (2007).

64. Schrieffer, J. & Wolff, P. Relation between the anderson and kondo hamiltonians. *Phys. Rev.* **149**, 491 (1966).

Acknowledgements

S.F. acknowledges support from the PRESTIGE program, under the Marie Curie Actions-COFUND of the FP7. G.R. acknowledges the support from the Fondo Nacional de Desarrollo Científico y Tecnológico (FONDECYT, Chile) under grant No. 1150653. E.S. acknowledges financial support from Spanish MINECO/FEDER FIS2015-69983-P and Basque Government IT986-16. Financial support by Fundación General CSIC (Programa ComFuturo) is acknowledged by C.S as well as additional support from Spanish MINECO/FEDER FIS2015-70856-P and CAM PRICYT Project QUITEMAD+ S2013/ICE-2801.

Author contributions statement

Must include all authors, identified by initials, for example:

Additional information

To include, in this order: **Accession codes** (where applicable); **Competing financial interests** (mandatory statement). The corresponding author is responsible for submitting a competing financial interests statement on behalf of all authors of the paper. This statement must be included in the submitted article file.

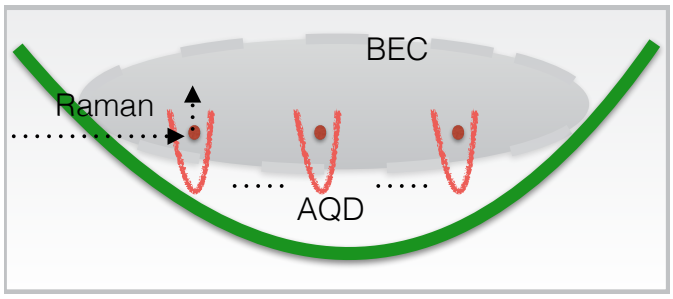

Figure 1. Schematic of the setup. Several atomic quantum dots (AQD) are coupled to the BEC atomic cloud in the superfluid regime by a Raman laser, which generates a phonon-mediated interaction.

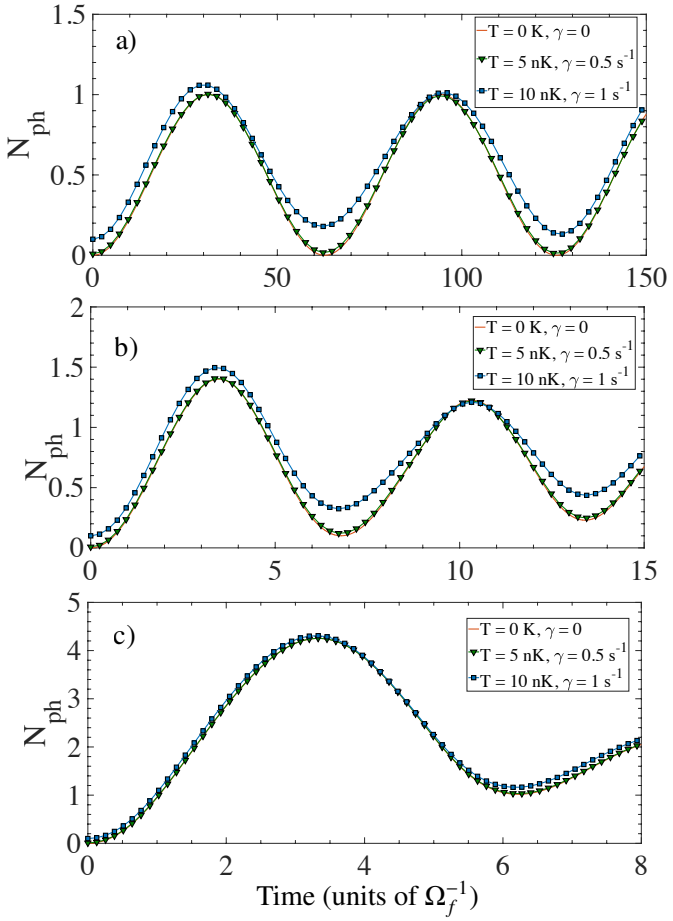

Figure 2. (Color online). Average photon number along time evolution, for different values of the coupling strength. a) $g = 0.05\ \Omega_f$, b) $g = 0.5\ \Omega_f$, and c) $g = \Omega_f$. In all plots, the TLS is taken to be resonant with the bosonic mode $\Omega_d = \Omega_f$. For all cases, the continuous red line corresponds to $T = 0$ nK and $\gamma = 0\ \mathrm{S}^{-1}$; for the inverted green triangles $T = 5$ nK and $\gamma = 0.5\ \mathrm{S}^{-1}$; finally, for the blue squares $T = 10$ nK and $\gamma = 1\ \mathrm{S}^{-1}$

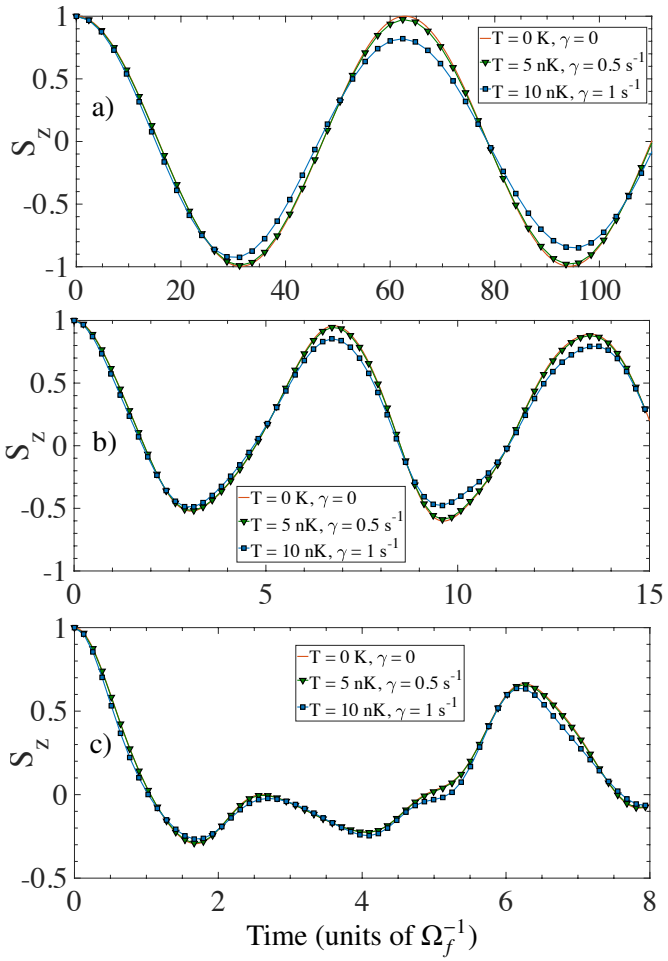

Figure 3. (Color online). Expected value of σ_z along time evolution, for different values of the coupling strength. a) $g = 0.05\ \Omega_f$, b) $g = 0.5\ \Omega_f$, and c) $g = \Omega_f$. In all plots, the TLS is taken to be resonant with the bosonic mode $\Omega_d = \Omega_f$. For all cases, the continuous red line corresponds to $T = 0$ nK and $\gamma = 0$ S^{-1}; for the inverted green triangles $T = 5$ nK and $\gamma = 0.5$ S^{-1}; finally, for the blue squares $T = 10$ nK and $\gamma = 1$ S^{-1}

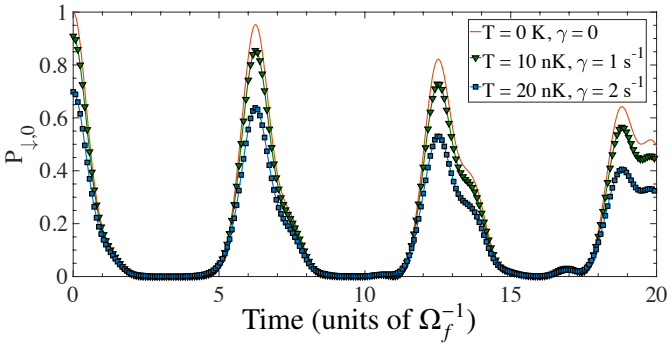

Figure 4. (Color online). Collapse and revival of the probability of finding the TLS in its ground state and the bosonic mode in the vacuum, during system time evolution. The initial state is given by the qubit ground state and a thermal state with temperature T for the bosonic mode. The qubit frequency is $\Omega_d = 0.8\ \Omega_f$. For both plots, the continuous red line corresponds to $T = 0$ nK and $\gamma = 0$ S^{-1}; for the green dashed line $T = 10$ nK and $\gamma = 1$ S^{-1}, and the blue dashed-dotted line for $T = 20$ nK and $\gamma = 2$ S^{-1}.

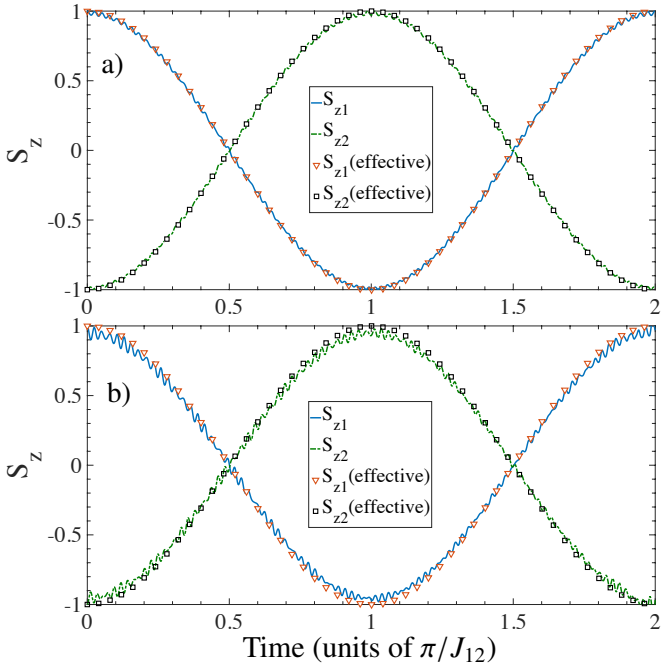

Figure 5. (Color online). Expected value of σ_z along time evolution. a) $T = 5$ nK and b) $T = 100$ nK. In all plots we consider $\Omega_f = 2\pi \times 10^3 \mathrm{s}^{-1}$, $\gamma = 1\mathrm{s}^{-1}$, and identical TLSs with parameters $\Omega_{d1} = \Omega_{d2} = 0.1\ \Omega_f$, and coupling strength $|g| = 0.054\ \Omega_f$. For all cases, the continuous blue line and the green dot-dashed lines correspond to the average value of σ_z for the first and second TLS respectively, when the full Hamiltonian (7) is considered. Inverted triangles and square markers correspond to the same observables, for the dynamics of the effective model (8).